BIOCHEMISTRY
including biophysical chemistry & molecular biology

Article

pubs.acs.org/biochemistry

Two Loops Undergoing Concerted Dynamics Regulate the Activity of the ASH1L Histone Methyltransferase

David S. Rogawski,[†] Juliano Ndoj,[†] Hyo Je Cho,[†] Ivan Maillard,[‡,§,∥] Jolanta Grembecka,[†] and Tomasz Cierpicki*[,†]

[†]Department of Pathology, [‡]Center for Stem Cell Biology, Life Sciences Institute, [§]Division of Hematology-Oncology, Department of Internal Medicine, and [∥]Department of Cell and Developmental Biology, University of Michigan, Ann Arbor, Michigan 48109, United States

Supporting Information

ABSTRACT: ASH1L (absent, small, or homeotic-like 1) is a histone methyltransferase (HMTase) involved in gene activation that is overexpressed in multiple forms of cancer. Previous studies of ASH1L's catalytic SET domain identified an autoinhibitory loop that blocks access of histone substrate to the enzyme active site. Here, we used both nuclear magnetic resonance and X-ray crystallography to identify conformational dynamics in the ASH1L autoinhibitory loop. Using site-directed mutagenesis, we found that point mutations in the autoinhibitory loop that perturb the structure of the SET domain result in decreased enzyme activity, indicating that the autoinhibitory loop is not a simple gate to the active site but is rather a key feature critical to ASH1L function. We also identified a second loop in the SET-I subdomain of ASH1L that experiences conformational dynamics, and we trapped two different conformations of this loop using crystallographic studies. Mutation of the SET-I loop led to a large decrease in ASH1L enzymatic activity in addition to a significant conformational change in the SET-I loop, demonstrating the importance of the structure and dynamics of the SET-I loop to ASH1L function. Furthermore, we found that three C-terminal chromatin-interacting domains greatly enhance ASH1L enzymatic activity and that ASH1L requires native nucleosome substrate for robust activity. Our study illuminates the role of concerted conformational dynamics in ASH1L function and identifies structural features important for ASH1L enzymatic activity.

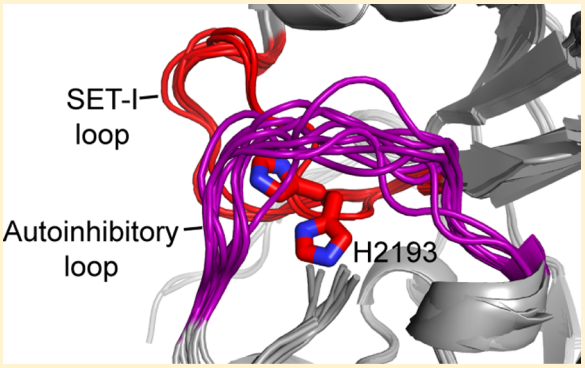

ASH1L (absent, small, or homeotic-like 1) is a mammalian homologue of Ash1, a member of the trithorax group of proteins essential for epigenetic mechanisms of gene activation.[1] ASH1L is a SET domain-containing histone methyltransferase (HMTase) with controversial substrate specificity. ASH1L was shown to methylate H3K4[2,3] and H3K36[4−8] in mammals. Although the specificity of the SET domain and function of ASH1L *in vivo* are not yet clear, emerging data link ASH1L to multiple cancers. In breast cancer, 27% of aggressive, basal-like breast cancers have high-level copy number amplifications of the *ASH1L* gene.[9] Moreover, high levels of ASH1L mRNA are associated with shorter survival in breast cancer patients.[9] In thyroid cancer, ASH1L is overexpressed in tumor-specific truncated forms and is downregulated by a tumor suppressor microRNA.[10] Amplifications of ASH1L are found in a variety of other tumors, such as lung and uterine cancer,[11,12] while mutations in ASH1L have been identified in gastric cancer,[13] colorectal cancer,[14] esophageal squamous cell cancer,[15] and lung cancer.[16] ASH1L activates genes in the *HOX-A*, *HOX-B*, and *HOX-C* clusters,[17,18] which are overexpressed in multiple cancers and correlated with metastasis and aggressive disease.[19] Notably, ASH1L activates *HOXA9* and its collaborator *MEIS1*,[18] which are oncogenes in leukemia.[20]

The ASH1L protein has a large and unannotated N-terminus, a SET domain responsible for HMTase activity, and three C-terminal chromatin-interacting domains: bromodomain, plant homeodomain (PHD), and bromo-associated homology (BAH) domain.[6] ASH1L's catalytic SET domain is required for its gene activating function, as deletion of the ASH1L SET domain in differentiating mouse embryonic stem cells leads to a decrease in the level of expression of multiple genes, including members of the *Wnt* and *Hox* families.[6] Most SET domains, including ASH1L SET, can be divided into four subdomains: associated with SET (AWS), core SET, post-SET, and the variable SET-I subdomain positioned in the middle of core SET, which is a putative substrate specificity cassette for HMTases.[21] In ASH1L and the closely related NSD1 and SETD2 HMTases, a region in the post-SET subdomain called the autoinhibitory loop blocks access of histone substrate to the enzyme active site.[7,22,23] It is unclear how the autoinhibitory loop reorients to accommodate substrate binding, as the structures for ASH1L, NSD1, and SETD2 were determined in

Received: June 22, 2015
Revised: August 19, 2015
Published: August 20, 2015

DOI: 10.1021/acs.biochem.5b00697
Biochemistry 2015, 54, 5401−5413

Table 1. Crystallographic Data Collection and Refinement Statistics for ASH1L WT and Mutants[a]

	ASH1L WT	ASH1L S2259M	ASH1L H2193F	ASH1L Q2265A	ASH1L K2264L
PDB entry	4YNM	4YNP	4YPE	4YPA	4YPU
Data Collection					
space group	$P3_221$	$P3_221$	$P3_221$	$P1$	$P3_221$
cell dimensions					
a, b, c (Å)	59.1, 59.1, 231.0	59.3, 59.3, 233.9	58.8, 58.8, 232.2	53.7, 61.8, 73.2	59.1, 59.1, 226.0
α, β, γ (deg)	90, 90, 120	90, 90, 120	90, 90, 120	91.6, 93.8, 90.5	90, 90, 120
no. protein molecules in the asymmetric unit	2	2	2	4	2
resolution (Å)	50−2.20 (2.24−2.20)	50−2.90 (2.95−2.90)	50−2.20 (2.24−2.20)	50−2.30 (2.34−2.30)	50−2.60 (2.64−2.60)
R_{merge} (%)	9.5 (59.0)	8.8 (39.3)	7.3 (38.5)	6.0 (25.5)	8.8 (48.3)
R_{meas} (%)	10.1 (62.6)	9.4 (41.7)	8.0 (41.6)	8.6 (36.2)	9.3 (51.0)
$CC_{1/2}$[b] in outer shell	0.87	0.93	0.92	0.85	0.94
$I/\sigma I$	33.7 (3.5)	25.2 (4.4)	24.4 (4.1)	15.5 (2.8)	42.2 (6.4)
completeness (%)	99.9 (100.0)	96.1 (96.0)	86.1 (79.5)	96.0 (97.3)	99.4 (98.2)
redundancy	9.1 (9.1)	7.7 (7.4)	5.2 (5.7)	2.0 (2.0)	9.1 (9.0)
Refinement					
resolution (Å)	46.82−2.20	47.00−2.90	42.56−2.20	73.04−2.30	75.35−2.60
no. of reflections	23762	10352	20191	38087	14072
no. of atoms	3497	3364	3572	7254	3373
protein	3333	3304	3405	6920	3277
SAM	54	54	54	108	54
Zn^{2+}	6	6	6	12	6
water	104	0	107	214	36
R_{work}, R_{free}	24.2, 27.8	26.2, 31.9	21.7, 26.3	24.9, 30.3	23.8, 30.5
average B factor	42.4	54.7	32.2	38.0	53.1
autoinhibitory loop	66.8	71.8	65.5	57.0	82.3
SAM	35.1	54.8	28.3	25.2	52.8
root-mean-square deviation					
bond lengths (Å)	0.017	0.006	0.022	0.018	0.013
bond angles (deg)	1.769	0.973	1.940	1.645	1.479
Ramachandran favored (%)	93.3	90.0	92.3	91.3	89.7
Ramachandran allowed (%)	5.7	9.0	7.5	7.5	8.5
Ramachandran outliers (%)	1.0	1.0	0.2	1.2	1.8
MolProbity clash score	11.86	4.74	10.7	16.6	7.41

[a]All diffraction data were obtained from a single crystal. Values in parentheses are for the highest-resolution shell. [b]$CC_{1/2}$ is the Pearson correlation coefficient of two half-data sets as defined by Karplus and Diederichs.[52]

the absence of histone substrate. Furthermore, whether the autoinhibitory loop functions simply as a gate to the active site or whether it forms important interactions with nucleosome substrates is unknown. In the case of NSD1, molecular dynamics simulations showed modest flexibility of the NSD1 autoinhibitory loop that may permit the H3K36 side chain to access NSD1's lysine binding channel,[22] but this computational study was not confirmed experimentally. In the case of SETD2, an open and substrate-accessible conformation of the autoinhibitory loop was observed by crystallographic studies upon binding of *N*-propyl sinefungin, which forces reorientation of Arg1670 that normally occupies the substrate lysine binding channel.[23] Even less is known about the function of the autoinhibitory loop of ASH1L. In the ASH1L SET domain crystal structure, high *B* factors for the autoinhibitory loop led the authors to conclude that this loop is highly mobile.[7] The functional significance of this mobility in solution, however, remains unclear. Interestingly, a Q2265A ASH1L mutant with increased catalytic activity had a highly disordered autoinhibitory loop as determined by preliminary structural analysis, suggesting that destabilization of the autoinhibitory loop might be sufficient to increase ASH1L enzymatic activity.[7]

Here we aimed to improve our understanding of the function of ASH1L by investigating structural features of the ASH1L SET domain and assessing how they regulate its HMTase activity. Using X-ray crystallography and nuclear magnetic resonance (NMR), we found that two loops surrounding the active site of ASH1L, the autoinhibitory loop and a loop in the SET-I subdomain, undergo concerted conformational dynamics. We designed several mutations in the SET domain to perturb the conformation of these loops and characterized the structure and activity of the mutants. We found that the autoinhibitory loop is not a simple gate blocking access to the active site. Instead, the autoinhibitory loop and the SET-I loop represent important structural features required for ASH1L SET domain activity. Moreover, our study emphasizes that concerted dynamics play a significant role in ASH1L HMTase activity. These results shed light on the mechanisms of SET

DOI: 10.1021/acs.biochem.5b00697
Biochemistry 2015, 54, 5401−5413

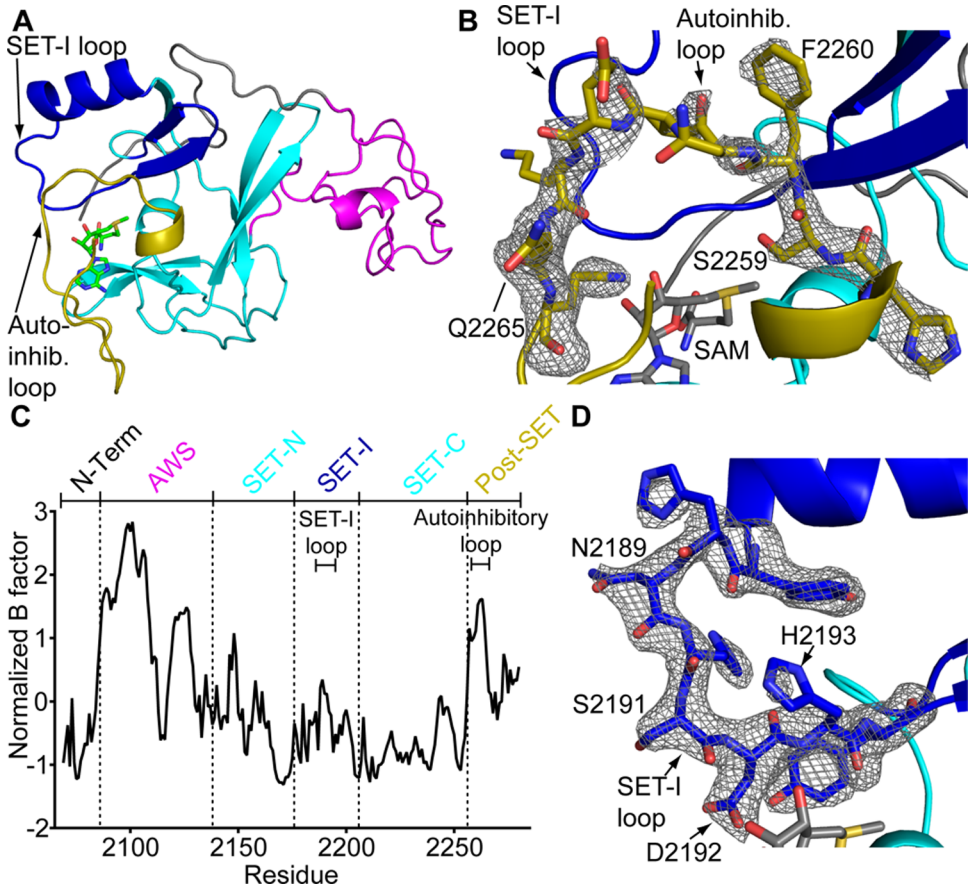

Figure 1. Analysis of the ASH1L SET domain crystal structure. (A) Cartoon representation of the ASH1L SET domain, colored by subdomain: N-terminus, gray; AWS, magenta; core SET, cyan; SET-I, blue; post-SET, dark yellow. (B) Autoinhibitory loop of ASH1L with the $mF_o - DF_c$ omit map contoured at 2.5σ. Subdomains colored as in panel A. (C) Normalized crystallographic *B* factors for the ASH1L SET domain. (D) SET-I loop of ASH1L with the $mF_o - DF_c$ omit map contoured at 2.5σ. Subdomains colored as in panel A.

domain function and may provide a foundation for the development of ASH1L inhibitors.

EXPERIMENTAL PROCEDURES

ASH1L Constructs. ASH1L SET (amino acids 2069−2288), ASH1L SET-PHD (amino acids 2069−2636), and ASH1L SET-BAH (amino acids 2069−2833) were cloned from the full length human *ASH1L* cDNA. ASH1L N-SET (amino acids 2003−2303) was codon-optimized for expression in *Escherichia coli*, and the DNA was purchased from Life Technologies. Point mutations were made in SET and SET-BAH constructs by polymerase chain reaction (PCR) and confirmed by DNA sequencing.

Protein Purification. ASH1L SET and N-SET proteins were expressed as MOCR fusion proteins in *E. coli* BL21(DE3) T1R cells at 22 °C. Transformed cells were lysed in buffer A containing 50 mM Tris (pH 7.5), 500 mM NaCl, 1 mM tris(2-carboxyethyl)phosphine (TCEP), and 20 mM imidazole. Cell debris was pelleted by centrifugation, and the supernatant was loaded on a column packed with nickel-nitrilotriacetic acid beads. The column was washed with buffer A and protein eluted with a 100 mL linear gradient up to buffer A containing 500 mM imidazole. The MOCR tag was cleaved with tobacco etch virus (TEV) protease during overnight dialysis against 50 mM Tris (pH 7.5), 100 mM NaCl, and 1 mM TCEP. Cleaved ASH1L was isolated from MOCR by repeating the nickel column purification and collecting ASH1L in the flow-through and low-imidazole fractions. ASH1L was further purified by gel filtration chromatography using a Superdex-75 column running in buffer B containing 50 mM Tris (pH 7.5), 100 mM NaCl, and 1 mM TCEP. ASH1L SET-PHD and SET-BAH proteins were purified similarly, with the following differences. Expression was performed at 18 °C; cleavage with TEV and the second nickel column were omitted to maintain protein stability, and gel filtration was performed on a Superdex-200 column.

Crystallization and Structure Determination. ASH1L wild-type and mutant SET domain proteins in buffer B were concentrated to 10 mg/mL. Crystals of ASH1L SET domain wild type as well as S2259M, K2264L, and H2193F mutants were obtained using the sitting drop method in 20 mM Tris (pH 7.5) and 25% PEG3350 at 4 °C. Q2265A crystals were obtained using the sitting drop method in 0.1 M Tris (pH 8.5), 0.2 M $MgCl_2$, and 30% PEG4000 at 17 °C. For cryoprotection, crystals of WT, S2259M, K2264L, and H2193F were soaked in a crystallization solution containing 20% glycerol, while Q2265A crystals were soaked in a crystallization solution containing 25% PEG400. All data were collected under cryogenic conditions at Life Sciences-Collaborative Access Team beamlines 21ID-D, -F, and -G at the Advanced Photon Source at Argonne National Laboratory (Argonne, IL). Data were processed with HKL2000.[24] Structures were determined by molecular replacement using MOLREP[25] with the wild-type ASH1L structure [Protein Data Bank (PDB) entry 3OPE] as a

DOI: 10.1021/acs.biochem.5b00697
Biochemistry 2015, 54, 5401−5413

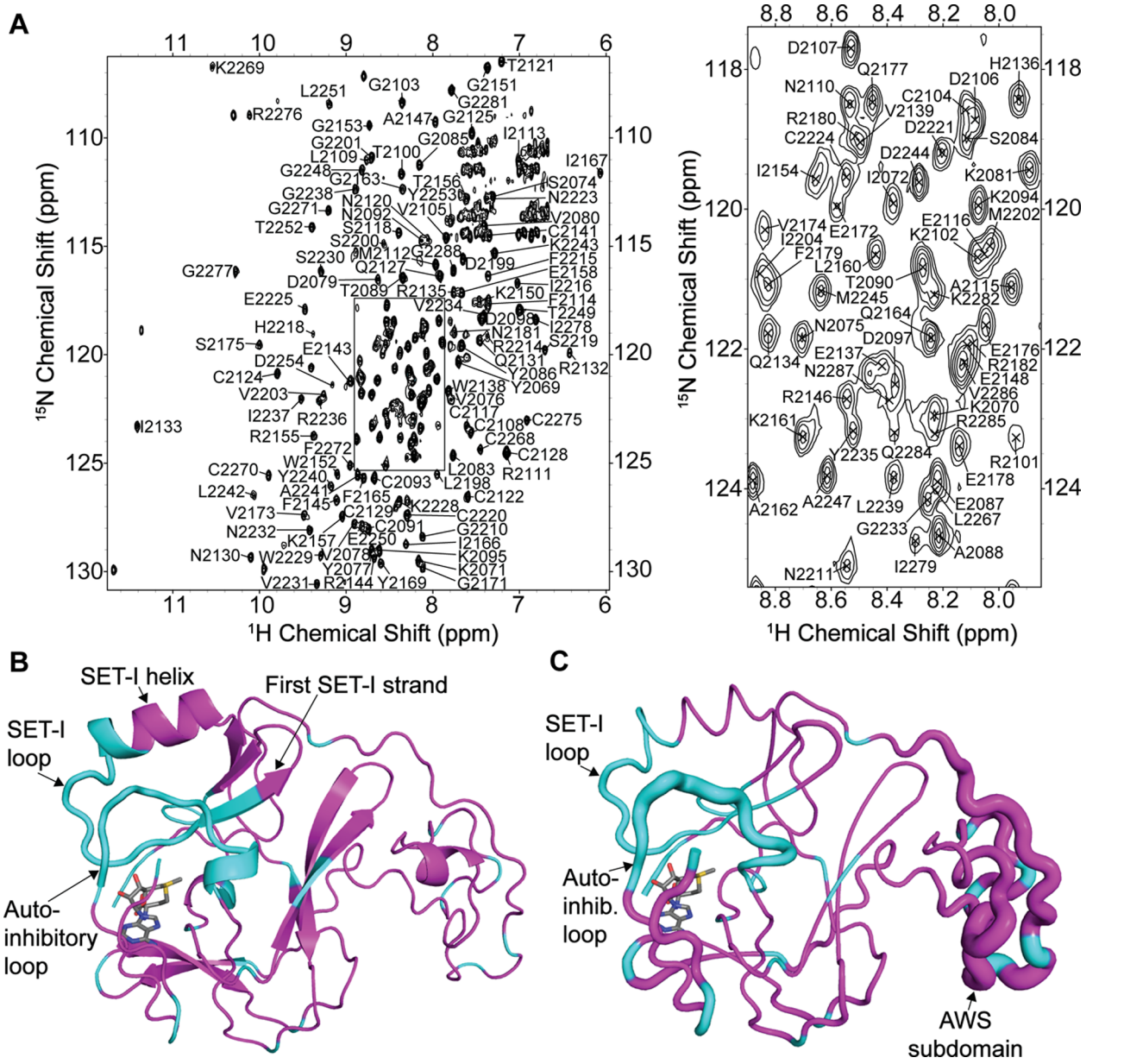

Figure 2. NMR studies of the ASH1L SET domain. (A) ^{15}N−^{1}H TROSY spectrum of the ASH1L SET domain with assignments. The right panel shows a close-up view of the central region of the spectrum. (B) NMR assignment mapped onto the ASH1L SET domain crystal structure. Residues with assigned peaks in the TROSY spectrum are colored magenta, while unassigned residues are colored cyan. (C) Cartoon putty representation of ASH1L with the thickness of cartoon being directly proportional to the *B* factor. Assigned and unassigned residues colored as in panel B.

search model in molecular replacement. Models were built and refined using REFMAC5,[26] *Coot*,[27] and the CCP4 package.[28] Validation of structures was performed using MolProbity.[29] Details of data processing and refinement are summarized in Table 1.

Average crystallographic *B* factors per residue were calculated as the average of the *B* factors for all the atoms of each residue. Then the residue *B* factors were normalized using the "*z*-score normalization"[30]

$$B_{x-z\text{-score}(i)} = [B_{x(i)} - \langle B\rangle_{(i)}]/s_{(i)} \quad (1)$$

where $B_{x\text{-zscore}(i)}$ is the normalized *z*-score for residue *x* in structure *i*, $B_{x(i)}$ is the *B* factor for residue *x*, $\langle B\rangle_{(i)}$ is the average residue *B* factor for structure *i*, and $s_{(i)}$ is the corresponding standard deviation.

NMR Studies. ^{15}N−^{13}C ASH1L SET was prepared at a concentration of 300 μM in buffer containing 50 mM HEPES (pH 7.5), 50 mM NaCl, 1 mM TCEP, and 300 μM *S*-adenosylmethionine (SAM). HSQC spectra were recorded at 25 and 30 °C with a Bruker Avance III spectrometer equipped with a cryoprobe, running Topspin version 2.1. Backbone assignment was performed using triple-resonance experiments: HNCA, HN(CO)CA, HNCACB, and CBCA(CO)NH. For analysis of ASH1L mutants, wild-type and mutant ASH1L SET proteins were prepared at a concentration of 100 μM in 50 mM Tris (pH 7.5), 50 mM NaCl, 1 mM TCEP, 200 μM SAM, 5% DMSO, and 5% D_2O. ^{1}H−^{15}N TROSY spectra were recorded at 30 °C. All NMR processing and spectral visualization were performed using NMRPipe[31] and Sparky.[32]

Chemical shift perturbations (Δ) in ^{15}N−^{1}H TROSY spectra caused by mutations compared to the wild type were calculated

DOI: 10.1021/acs.biochem.5b00697
Biochemistry 2015, 54, 5401−5413

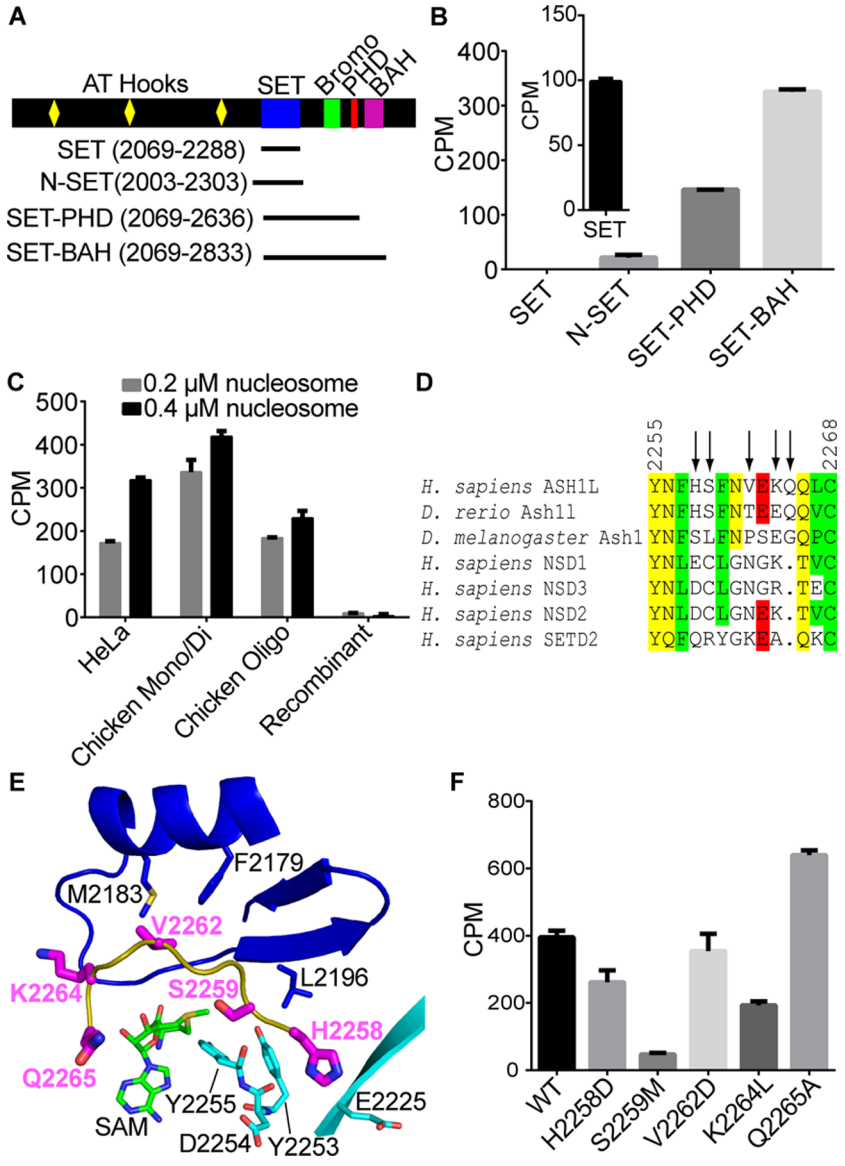

Figure 3. Enzymatic activity of ASH1L variants. (A) Schematic of ASH1L variants tested in the enzymatic assay. (B) Activity in counts per minute (cpm) of ASH1L constructs with chicken mono/dinucleosome substrate at 0.25 μM ASH1L and 0.2 μM nucleosome. The inset shows the activity of ASH1L SET at 1 μM enzyme and 0.8 μM nucleosomes. (C) Activity of the ASH1L SET-BAH construct with various native and recombinant nucleosome substrates at 0.2 or 0.4 μM. (D) Sequence alignment of the autoinhibitory loop of human ASH1L with related HMTases. Sites selected for mutagenesis are denoted with arrows. (E) Location of residues selected for mutagenesis (magenta). (F) Activity of ASH1L SET-BAH WT and mutant proteins on chicken mono/dinucleosomes using 0.25 μM ASH1L and 1.7 μM chicken mono/dinucleosomes.

as the square root of the sum of the squares of the differences in the ^{1}H and ^{15}N chemical shifts[33]

$$\Delta = [(\delta_H \times 600)^2 + (\delta_N \times 60.8)^2]^{1/2} \quad (2)$$

where δ_H and δ_N are the chemical shift differences in parts per million between the mutant and wild type for ^{1}H and ^{15}N, respectively. Global structural perturbations caused by mutations were determined by calculating the sum of Δ for all amides (Δ_{sum}).

Histone Methyltransferase Assay. Chicken mono/dinucleosomes (HMT-35-179), chicken oligo nucleosomes (HMT-35-177), and HeLa nucleosomes (HMT-35-123) were purchased from Reaction Biology. Recombinant nucleosomes were purified in house as described previously.[34] For testing different ASH1L constructs and nucleosome substrates, ASH1L (0.25 μM) was incubated with 0.7 μM SAM and 0.2 or 0.4 μM nucleosome in HMTase buffer containing 50 mM Tris (pH 8.5), 25 mM NaCl, 2 mM $MgCl_2$, and 1 mM DTT in a total volume of 25 μL for 1 h at 30 °C. For assays with ASH1L mutants, ASH1L WT and mutant proteins (0.25 μM) were incubated with 20 μM SAM (5% radiolabeled [^{3}H]SAM) and 1.7 μM chicken mono/dinucleosomes in HMTase buffer in a total volume of 10 μL for 1 h at 30 °C. The reactions were stopped by spotting 5 μL of the reaction mixture on P81 phosphocellulose squares (Millipore). The P81 squares were dried for 45 min and washed five times with 50 mM sodium bicarbonate (pH 9.0), 10 min per wash. The P81 squares were then dried for 1 h, added to 10 mL of Ultima Gold scintillation cocktail (PerkinElmer), and analyzed using a Beckman scintillation counter.

DOI: 10.1021/acs.biochem.5b00697
Biochemistry 2015, 54, 5401−5413

RESULTS

The Crystal Structure of the ASH1L SET Domain Shows Increased Dynamics of the Autoinhibitory and SET-I Loops. To gain insight into the mechanism of methyltransferase activity by ASH1L, we determined the crystal structure of the ASH1L SET domain (residues 2069−2288) (Figure 1A). The crystals diffracted to 2.2 Å resolution, representing a significant improvement over the previously published 2.9 Å structure of the ASH1L SET domain.[7] The higher resolution allowed us to more precisely model residues throughout the structure, including regions associated with the catalytic activity of ASH1L. We observed satisfactory electron density for the main chain and for the majority of side chains in the autoinhibitory loop (residues 2258−2266) (Figure 1B). The poor electron density for some side chains suggested that the autoinhibitory loop may experience conformational dynamics, and to further evaluate dynamics of the SET domain, we used crystallographic *B* factors. We found that the autoinhibitory loop and the AWS region have the highest *B* factors, suggesting that these are more mobile regions (Figure 1C). Interestingly, we also found that the SET-I subdomain has *B* factors higher than those of the neighboring C-terminal core SET region (SET-C) (Figure 1C). The SET-I subdomain consists of a helix−loop−strand−turn−strand motif, with the SET-I loop (residues 2187−2195) in this motif located directly beneath the autoinhibitory loop (Figure 1D). Residues 2192−2194 in the SET-I loop make both polar and hydrophobic contacts with the *S*-adenosylmethionine (SAM) cofactor. We observed well-defined electron density for SET-I residues, with the exception of the side chain of His2193, which is poorly defined, indicating that this residue may undergo conformational exchange (Figure 1D).

NMR Studies Reveal That the ASH1L Active Site Is Surrounded by Two Loops Experiencing Conformational Dynamics. To further investigate the dynamics of the ASH1L SET domain, we performed NMR studies in solution. We collected a $^{15}N-^{1}H$ TROSY NMR spectrum for the ASH1L SET domain. While the ASH1L SET construct contains 213 non-proline residues, we observed only 181 backbone amide peaks in the NMR spectrum. The large number of missing peaks suggested that a significant portion of the protein is undergoing intermediate exchange dynamics on the microsecond to millisecond time scale.[35,36] To identify the regions undergoing such dynamics, we completed backbone assignments based on triple-resonance experiments for ^{15}N- and ^{13}C-labeled ASH1L (Figure 2A). We were able to assign 168 (93%) of the 181 peaks observed for backbone amides. Interestingly, we were not able to observe any backbone amide peaks for residues in the autoinhibitory loop and in a large portion of the SET-I subdomain, including the entire SET-I loop, while we obtained nearly complete assignment for the remaining part of the SET domain (Figure 2A,B). This observation strongly suggests that the autoinhibitory and SET-I loops surrounding the active site of ASH1L experience conformational dynamics, in agreement with crystallographic data presented above. Interestingly, while the crystallographic *B* factors for the AWS subdomain are very high, we observe nearly all the AWS residues in the NMR spectrum (Figure 2C), suggesting that in solution the AWS subdomain undergoes dynamics on a time scale much faster than that of the SET-I loop and autoinhibitory loop. Overall, we concluded that two loops surrounding the active site of ASH1L, the autoinhibitory loop and the SET-I loop, are undergoing dynamics in solution on the microsecond to millisecond time scale.

ASH1L Requires Chromatin-Interacting Domains for Robust Enzymatic Activity. We next aimed to develop a robust assay to measure the catalytic activity of ASH1L. A previous study showed weak catalytic activity for the isolated SET domain of ASH1L.[6] We tested the catalytic activity of ASH1L SET in a radiometric HMTase assay with different substrates, including chicken nucleosomes, and detected weak activity using 1 μM ASH1L SET construct (Figure 3A) and 0.8 μM nucleosomes (Figure 3B, inset). Because full length ASH1L is a large multidomain protein with three chromatin-interacting domains at its C-terminus (a bromodomain,[37] a PHD finger,[38] and a BAH domain[39]) (Figure 3A), we wondered whether these domains would enhance ASH1L HMTase activity.

To investigate the effect of the chromatin-interacting domains on ASH1L HMTase activity, we designed three additional ASH1L constructs of different lengths systematically incorporating the chromatin reader domains at the C-terminus of the protein (Figure 3A). We tested the enzymatic activity of the different ASH1L constructs using 0.25 μM ASH1L and 0.2 μM chicken mono/dinucleosome substrate. We found that the isolated SET domain has no detectable HMTase activity on chicken nucleosome substrate under these assay conditions (Figure 3B). A larger construct incorporating the N-terminal flanking region of the SET domain (N-SET)[6] also had very low activity (Figure 3B). In contrast, the SET-PHD and SET-BAH constructs had significantly higher HMTase activity, with the longest construct SET-BAH being most active (Figure 3B). These results show that chromatin-interacting domains are necessary for robust enzymatic activity of ASH1L, likely through recruitment of nucleosome substrates. Despite the significantly enhanced activity, we were not able to characterize kinetic parameters for ASH1L because the signal was too weak at the low nanomolar enzyme concentrations required to accurately determine the Michaelis constants.

ASH1L SET-BAH Requires Native Nucleosome Substrate for Optimal Enzymatic Activity. Previous studies have shown that ASH1L requires nucleosomes as the substrate,[6,7] and a recent study by Eram et al. showed enhanced activity of the ASH1L SET domain on native chicken nucleosomes compared to its activity on recombinant, reconstituted nucleosomes.[8] We tested whether our longer, most active ASH1L SET-BAH construct also has enhanced activity on native versus recombinant nucleosomes. We found that, indeed, SET-BAH had much higher activity on native nucleosomes (Figure 3C). Interestingly, among the native nucleosomes we tested, ASH1L SET-BAH exhibited nearly 2-fold higher activity on chicken mono/dinucleosomes than HeLa nucleosomes and chicken oligonucleosomes at a nucleosome concentration of 0.2 μM (Figure 3C). Taken together with the results of Eram et al., our studies indicate that ASH1L exhibits greater activity on native nucleosomes, and this may be partly due to recognition of covalent modifications on native nucleosomes through the chromatin-interacting domains of ASH1L.

Mutations of Nonconserved Residues in the Autoinhibitory Loop Have Significant Effects on ASH1L SET Domain Activity. A previous study suggested that the autoinhibitory loop of ASH1L regulates its HMTase activity, likely by physically blocking access to the active site.[7] On the other hand, our results indicated that the autoinhibitory and SET-I loops surrounding the active site of the SET domain

DOI: 10.1021/acs.biochem.5b00697
Biochemistry 2015, 54, 5401−5413

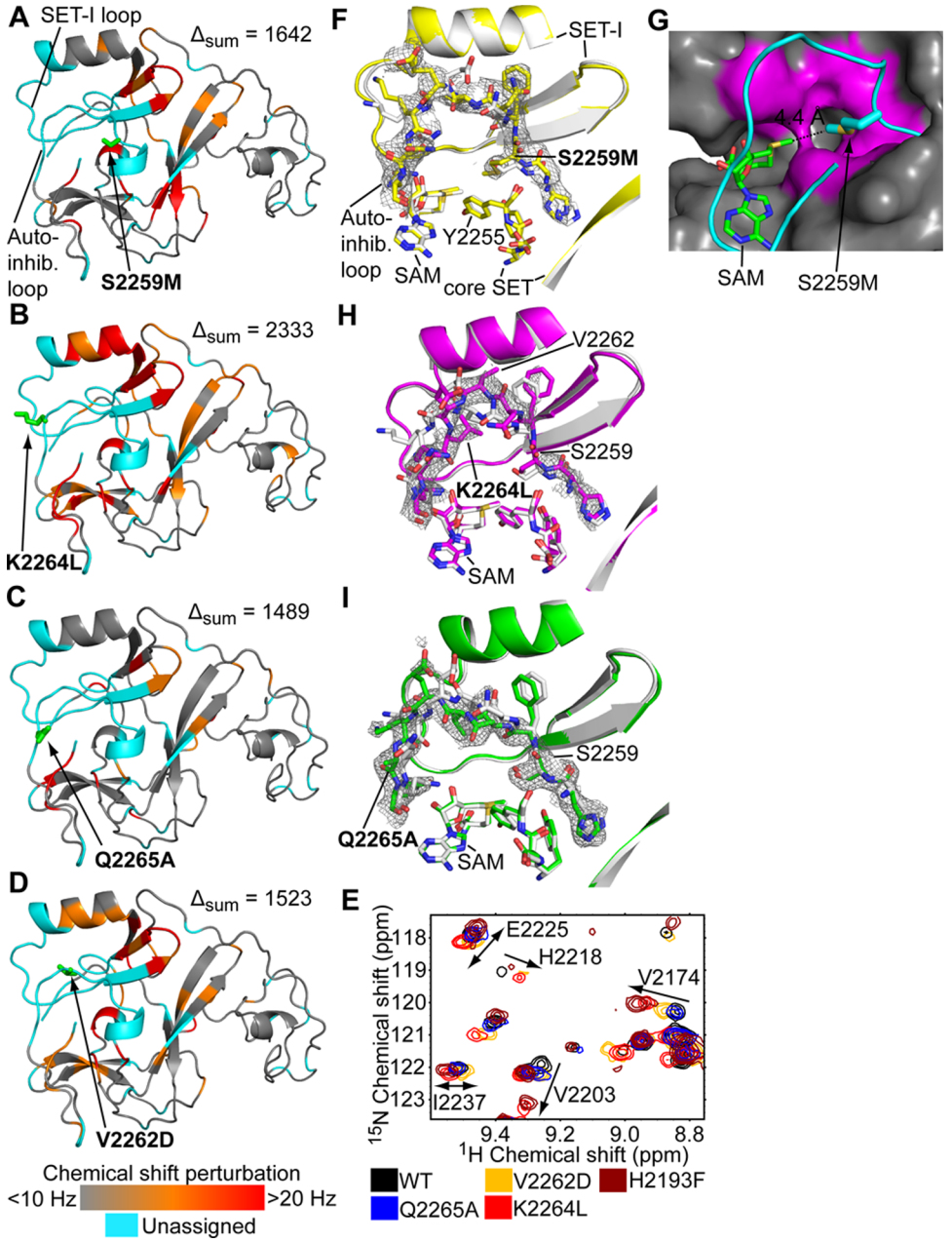

Figure 4. Effects of autoinhibitory loop mutations in ASH1L. (A–D) Chemical shift perturbations (Δ; see Experimental Procedures) of backbone amides in TROSY spectra induced by S2259M, K2264L, Q2265A, and V2262D mutations, respectively, mapped onto the crystal structure of the wild-type ASH1L SET domain: residues perturbed by <10 Hz, gray; residues perturbed by 10–20 Hz, orange; residues perturbed by ≥20 Hz, red; unassigned, cyan. Mutated residues are labeled and colored green. The sum of all chemical shift perturbations (Δ_{sum}) is shown for each mutant. (E) Regions of the TROSY spectra showing greater chemical shift perturbations caused by the K2264L and H2193F mutants. (F, H, and I) Comparison of the autoinhibitory loop conformation between the mutants [S2259M in yellow (F), K2264L in magenta (H), and Q2265A in green (I)] and wild-type ASH1L (gray), with $2mF_o - DF_c$ maps for the mutants contoured at 0.8σ. (G) Mutant Met2259 partially occupies the substrate lysine binding channel. The post-SET subdomain is depicted as a cartoon; all other regions depicted as surfaces. Residues His2193, Tyr2194, Cys2195, Leu2196, Tyr2253, and Tyr2255 that form the substrate lysine binding channel are colored magenta.

experience significant dynamics in solution. In addition, sequence analysis of SET domains related to human ASH1L indicates that residues in the autoinhibitory loop are not conserved (Figure 3D). We aimed to dissect the contribution of different residues in the autoinhibitory loop to the enzymatic activity of ASH1L by making a series of point mutations based on our crystal structure of the SET domain (Figure 3E and Figure S1). We explored rather severe mutations with the overall goal of affecting the conformation of the autoinhibitory loop while avoiding global disruption of the SET domain.

In an attempt to destabilize the autoinhibitory loop, we mutated His2258 to Asp to introduce electrostatic repulsion with two adjacent acidic residues, Glu2225 and Asp2254 (Figure 3E). Interestingly, we found that the H2258D mutant exhibited a modest ∼30% decrease in activity (Figure 3F), suggesting that electrostatic interactions involving His2258 play a minor role in regulating enzyme activity. Next we investigated the neighboring residue Ser2259, whose side chain points toward the *S*-methyl group of the SAM cofactor. Crystallographic studies of the related SETD2 HMTase suggested that

DOI: 10.1021/acs.biochem.5b00697
Biochemistry 2015, 54, 5401–5413

the amino acid occupying this position could play a key role in flipping the autoinhibitory loop from a closed to open conformation.[23] To investigate the regulatory potential of Ser2259, we mutated it to Met to enhance hydrophobic contacts with core SET and SET-I. We found that the S2259M mutation strongly decreased ASH1L activity by ∼90% (Figure 3F), consistent with an important regulatory role for Ser2259.

In the middle of the autoinhibitory loop, Val2262 forms hydrophobic contacts with Phe2179 and Met2183 in SET-I. To explore the role of these contacts, we mutated Val2262 to Asp. We found that the V2262D mutation caused nearly no effect on enzymatic activity compared to that of wild-type ASH1L (Figure 3F). This result suggests that the hydrophobic contacts made by Val2262 are not critical for enzymatic activity. The result is also consistent with the dynamic nature of the autoinhibitory loop, which may contact SET-I in only a subset of its heterogeneous conformations.

At the end of the autoinhibitory loop, we tested whether we could stabilize the autoinhibited form of the SET domain by mutating Lys2264 to Leu and thereby enhance hydrophobic contacts between the autoinhibitory loop and SET-I. The K2264L mutation decreased activity by ∼50% (Figure 3F), which is consistent with a need for polar residues at this position based on sequence alignment with related methyltransferases (Figure 3D). Finally, it was previously reported that mutation of the solvent-exposed Gln2265 to Ala results in the enhancement of ASH1L activity, likely through destabilization of the autoinhibitory loop.[7] To further explore this finding, we introduced the Q2265A mutation into the SET-BAH construct and found that indeed its activity is increased by ∼50% compared to that of the wild type (Figure 3F). Altogether, we found that despite their low-level conservation, the mutated autoinhibitory loop residues confer significant regulatory control over ASH1L enzyme activity. Our results suggest that the ASH1L autoinhibitory loop is a precisely tuned structural feature with a role more complex than simply blocking the active site.

NMR Studies Correlate the Degree of Structural Perturbation to Enzyme Activity. We used NMR to assess structural perturbations to the ASH1L SET domain caused by the autoinhibitory loop mutations. For these studies, we selected four mutants: S2259M, V2262D, K2264L, and Q2265A. We collected $^{15}N-^{1}H$ TROSY spectra for all four variants and mapped the chemical shift perturbations caused by the mutations onto the ASH1L crystal structure (Figure 4A–D). We found that both the S2259M and K2264L mutations caused perturbations to an area surrounding the dynamic autoinhibitory loop region of the protein (Figure 4A,B). The S2259M mutation caused chemical shift perturbations mostly in β-sheets in the SET-I region and core SET region that contact the autoinhibitory loop (Figure 4A). The K2264L mutation caused a greater number of perturbations in a complete shell surrounding the autoinhibitory loop (Figure 4B). In addition to the β-sheets affected by S2259M, the perturbed shell includes the SET-I helix and the C-terminal tail of the post-SET region, which are located above and below the autoinhibitory loop, respectively. The widespread chemical shift perturbations caused by single-amino acid substitutions in the autoinhibitory loop suggest regulatory cross-talk between the autoinhibitory loop and the rest of the SET domain.

Interestingly, we found that the Q2265A mutation, which was previously reported to destabilize the substrate-unbound conformation of the autoinhibitory loop,[7] led to very few chemical shift perturbations on the NMR spectrum of ASH1L (Figure 4C). Chemical shift perturbations were limited mostly to a small local area immediately adjacent to the Q2265A mutation, including residues in the post-SET subdomain. Finally, the V2262D mutation, which had nearly no effect on enzyme activity, also had a relatively weak effect on the structure of the SET domain as determined by NMR chemical shift perturbations (Figure 4D). Notably, we did not observe an increase in the total number of signals observed in the $^{15}N-^{1}H$ TROSY spectra for any of the mutants. Therefore, none of these mutations significantly alters the intermediate exchange dynamics in the autoinhibitory and SET-I loops.

In summary, our NMR analysis showed that mutations leading to large decreases in enzyme activity (S2259M and K2264L) caused significant structural perturbations throughout the SET domain. In contrast, mutations that had no effect or caused enhanced activity (V2262D and Q2265A) caused only small perturbations to the SET domain as measured by chemical shift perturbations (Figure 4A–E). These results suggest that the proper structure and dynamic properties of the ASH1L autoinhibitory loop are required for enzyme activity.

Mutations Affect the Structure and Mobility of the ASH1L Autoinhibitory Loop. Next we determined the crystal structures of the ASH1L SET domain mutants that caused the largest changes in activity: S2259M, K2264L, and Q2265A. After refinement of these structures, the R_{free} statistic remained high (Table 1), primarily because of the more flexible AWS subdomain. Compared to the WT structure, the S2259M structure showed modest changes to autoinhibitory loop side chains (Figure 4F). However, the side chain of Met2259 in the mutant protrudes into a channel bordered by the backbone atoms of His2193, Tyr2194, and Cys2195 and the side chains of Leu2196, Tyr2253, and Tyr2255, which is the putative substrate lysine binding site (Figure 4F,G). The Met2259 side chain methyl group is a short 4.4 Å distance from the *S*-methyl group of SAM. These data indicate that the profound reduction in activity of the S2259M mutant (Figure 3F) is likely caused by stabilization of the inactive conformation of the SET domain via interaction of the methionine side chain with the substrate lysine binding channel. Therefore, our findings suggest that Ser2259 is an important gatekeeper residue that partially occupies the lysine binding channel in the autoinhibited conformation of the SET domain.

In the K2264L structure, we observed intraloop hydrophobic contacts between Leu2264 and Val2262 (Figure 4H), rather than contacts with SET-I that we had designed to stabilize the loop. The new intraloop interaction between Leu2264 and Val2262 distorts the loop and disrupts the interaction between the autoinhibitory loop and SET-I subdomain. These results suggest that the ∼50% reduced activity of the K2264L mutant is caused by perturbations to the structure of the autoinhibitory loop. Interestingly, we observed very high *B* factors for the K2264L autoinhibitory loop (Table 1), indicating that despite new contacts between Leu2264 and Val2262 the loop has enhanced dynamics relative to that of WT ASH1L. These observations further support the conclusion that disruption of the structure and dynamic properties of the autoinhibitory loop is detrimental to enzyme activity.

The crystal structure of the hyperactive Q2265A mutant shows only minor differences in the conformation of the autoinhibitory loop as compared to that of the wild-type protein (Figure 4I), in agreement with the minimal effect of the Q2265A mutation on the NMR spectrum. In addition,

DOI: 10.1021/acs.biochem.5b00697
Biochemistry 2015, 54, 5401−5413

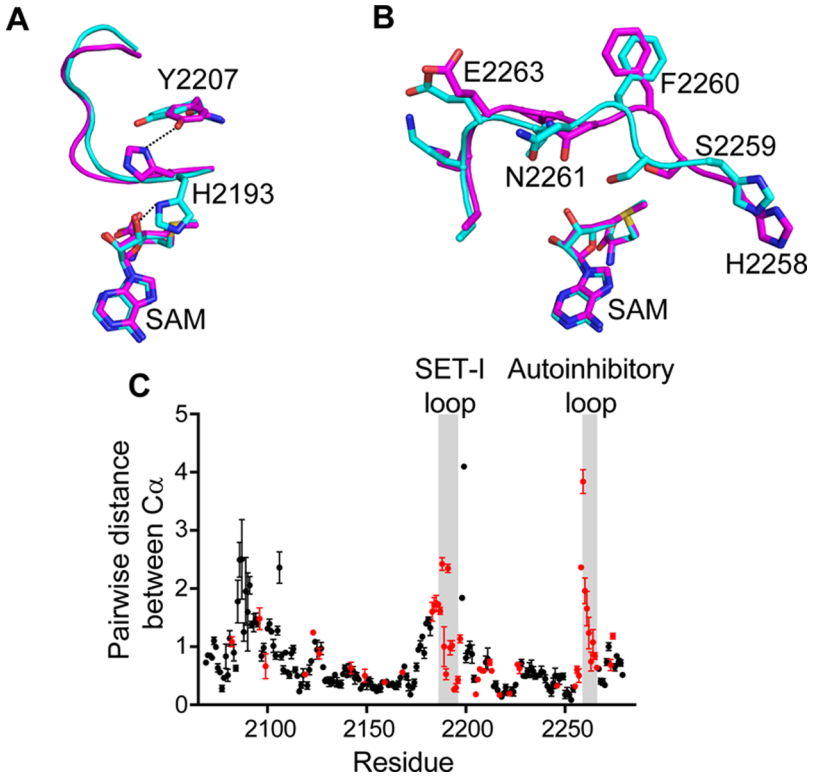

Figure 5. Conformational dynamics observed in the crystal structure of Q2265A. (A) Superposition of SET-I loops for two different ASH1L molecules in the asymmetric unit. His2193 can form a hydrogen bond either with the 3′-hydroxyl group of SAM or with the side chain of Tyr2207. (B) Superposition of autoinhibitory loops for two different ASH1L molecules in the asymmetric unit. (C) Pairwise distances between α-carbons for the two ASH1L conformations observed in the Q2265A crystal. SET-I and autoinhibitory loop regions are highlighted by gray fields, and residues unassigned in NMR spectra are colored red.

crystallographic *B* factors for the Q2265A autoinhibitory loop are comparable to those of the wild type (Table 1). Although it is possible, we did not observe evidence that different crystal packing of the Q2265A mutant artificially constrained the loop's mobility. Therefore, our Q2265A structure suggests that the enhanced activity of the Q2265A mutant may not be correlated with disordering of the autoinhibitory loop as previously suggested,[7] but a cocrystal structure of ASH1L with nucleosomes would be required to fully explain the effect of the Q2265A mutation. Finally, for all the mutants, we did not find evidence that altered SAM binding contributed to changes in enzymatic activity, as there were no significant differences in SAM orientation or *B* factor relative to the structure's average *B* factor (Table 1).

Structural Insight into SET-I Loop Conformational Dynamics. We found that the Q2265A mutant crystallized in a crystal form (*P*1) different from those of the other ASH1L variants ($P3_221$) (Table 1). There are four ASH1L Q2265A molecules per asymmetric unit, and interestingly, the Q2265A crystal traps two different conformations of the SET-I and autoinhibitory loops, with each conformation represented by a pair of ASH1L monomers (Figure 5A,B). The most interesting difference between the two conformations is the two orientations of His2193, with the histidine side chain forming a hydrogen bond either with the 3′-hydroxyl group of SAM or with the hydroxyl of Tyr2207 (Figure 5A). Such conformational exchange is consistent with the WT structure, in which we observe poor electron density for His2193 (Figure 1C). Thus, the structure of the Q2265A mutant provides snapshots of two different conformations of the SET-I loop. We also observed significant differences in the autoinhibitory loop between the two different ASH1L conformations (Figure 5B), further emphasizing the conformational dynamics of this loop.

We tested whether the Q2265A crystal structure could be used to corroborate the dynamics in ASH1L that we observed by NMR. We plotted pairwise distances between Cα positions for the two different ASH1L conformations observed in the crystal structure of this mutant. Compared to the rest of the core SET domain, we observed large structural differences for the SET-I and autoinhibitory loops (Figure 5C). The two molecules in the asymmetric unit of WT ASH1L also show structural differences for these loops, but the differences between molecules in the asymmetric unit are more significant and better resolved in the Q2265A mutant. Interestingly, residues that show these large structural differences are not observed in the NMR spectrum of the SET domain (both WT and Q2265A mutant). Therefore, intermediate dynamics that lead to broadening of NMR signals are consistent with conformational heterogeneity observed in the crystal structure of Q2265A.

Conformational Exchange in the SET-I Loop Contributes to ASH1L Activity. Analysis of the crystal structure of WT and Q2265A ASH1L indicated that the SET-I loop samples different conformations. We expected that such conformational heterogeneity might be partially regulated by His2193, which we found in two different conformations (Figure 5A). To probe the role of H2193, we introduced an H2193F mutation to disrupt its potential to form hydrogen bonds. We found that the H2193F mutation decreases activity of SET-BAH by >80% (Figure 6A). NMR studies of ASH1L

DOI: 10.1021/acs.biochem.5b00697
Biochemistry 2015, 54, 5401−5413

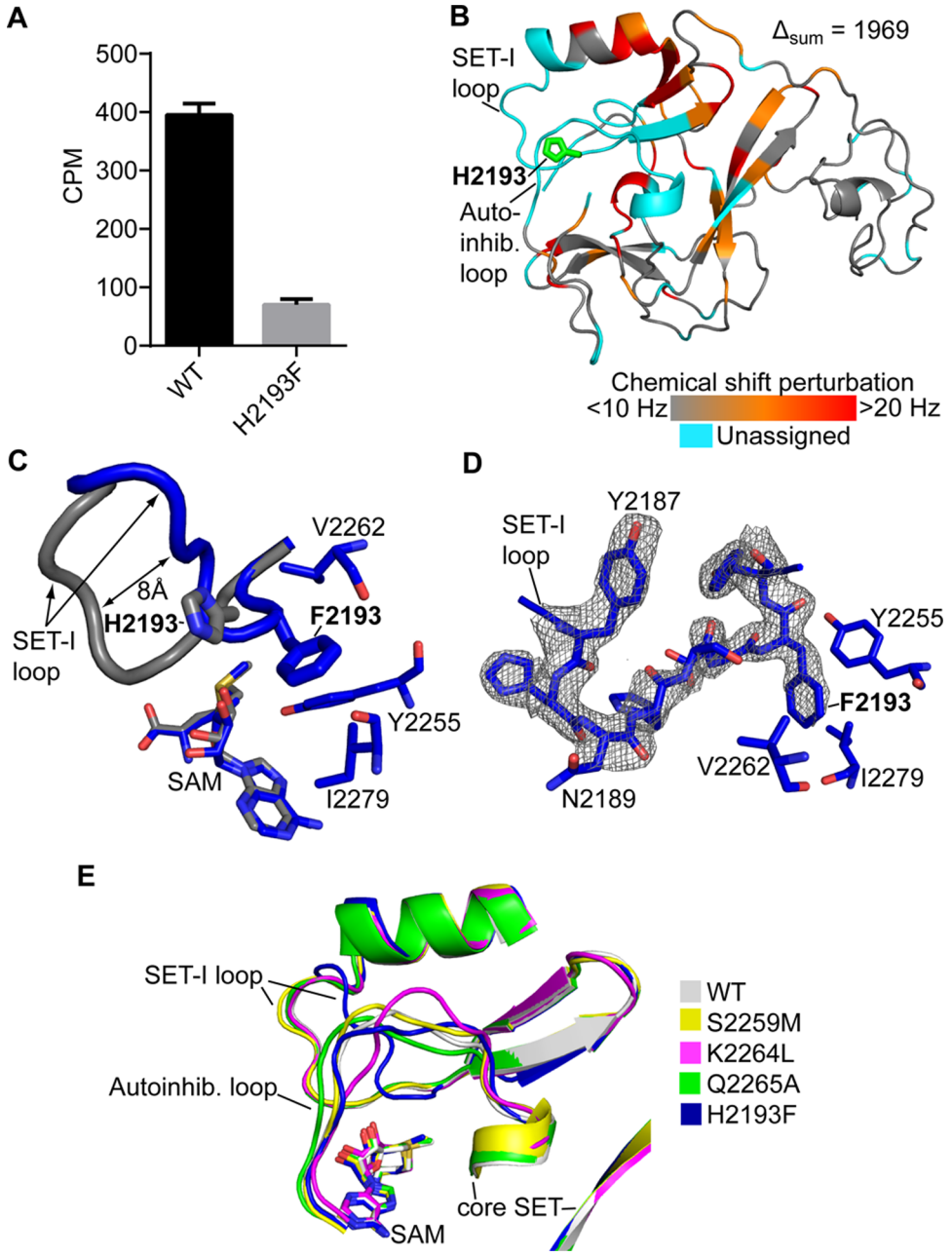

Figure 6. Structural perturbation in the SET-I loop induced by the H2193F mutation. (A) Enzymatic activity of wild-type and H2193F ASH1L with 0.25 μM ASH1L and 1.7 μM chicken mono/dinucleosome substrate. (B) Chemical shift perturbations in TROSY spectra induced by H2193F, color coding as in Figure 4. (C) Superposition of the SET-I loops of H2193F (blue) and the wild type (gray). Residues involved in hydrophobic contacts with Phe2193 are shown and labeled. (D) SET-I loop of the H2193F mutant with the $mF_o - DF_c$ omit map contoured at 2.5σ. Residues forming hydrophobic contacts with Phe2193 are shown. (E) Superposition of crystal structures of WT ASH1L and four mutants.

H2193F showed that the mutation causes widespread chemical shift perturbations extending in a shell surrounding the dynamic SET-I and autoinhibitory loops (Figure 6B). We determined the crystal structure of H2193F and found a large ~8 Å conformational shift in the SET-I loop, with minimal perturbations to other regions when compared to the wild-type protein (Figure 6C). Phe2193 in this mutant forms new hydrophobic contacts with Tyr2255, Val2262, and Ile2279 (Figure 6C,D). Interestingly, despite the significantly different conformation of the SET-I loop, the conformation of the autoinhibitory loop is unaffected. Altogether, these results demonstrate that conformational dynamics of the SET-I subdomain also play a significant role in modulating the catalytic activity of the ASH1L SET domain. Furthermore, the dynamics of the SET-I subdomain occur in concert with those of the autoinhibitory loop (Figure 6E) to affect regulation of enzymatic activity.

DISCUSSION

SET domain-containing HMTases make up an important class of enzymes that constitute attractive targets for new therapeutics,[40] but many structural aspects of SET domains remain poorly understood. The autoinhibitory loop is a striking feature observed in the crystal structure of the ASH1L SET domain. However, whether the loop functions as a simple swinging gate to allow access to the active site, or instead plays

DOI: 10.1021/acs.biochem.5b00697
Biochemistry 2015, 54, 5401−5413

a more active role in substrate binding, is unknown. In this study, we provide experimental evidence supporting the latter model. First, point mutations that destabilize the autoinhibitory loop did not increase enzymatic activity, as would be expected if the loop simply blocks access for substrate binding. Second, point mutations in the autoinhibitory loop that cause larger structural perturbations in the SET domain as judged from NMR and crystallography caused a substantial loss of enzyme activity, while point mutations that had weaker effects on the structure caused no change or even resulted in an increase in enzymatic activity compared to that of wild-type ASH1L. This suggests that the proper structure of the autoinhibitory loop is necessary for substrate binding, and the loop itself represents an important regulatory feature of the SET domain.

We discovered that in addition to the autoinhibitory loop, the SET-I loop plays an important role in ASH1L SET domain function. The dynamics of this conformationally heterogeneous loop are partly regulated by His2193, a residue in the SET-I loop that adapts two different conformations and mutation of which significantly impairs enzymatic activity. In other SET domain-containing proteins, the SET-I region is poorly conserved and forms key contacts with histone substrates,[21,41−44] indicating that it likely functions in determining substrate specificity among different HMTases.[45] In the structure of the related Pr-Set7 HMTase bound to a histone H4 fragment, the SET-I loop forms extensive contacts with the H4 peptide.[21,41] Our results indicate that SET-I is also important to the enzymatic activity of ASH1L, likely through forming analogous contacts with histone H3 residues.

Crystallographic and NMR studies of the SET domain and multiple mutants showed that the autoinhibitory loop and SET-I loop experience conformational dynamics occurring on the microsecond to millisecond time scale. Importantly, this conformational heterogeneity experienced in the absence of bound substrate does not appear to include an open, substrate-accessible form of the SET domain. The fully open conformation of ASH1L would require a conformational change much larger than any we observed, and most likely, such a conformation can be achieved in the presence of nucleosomes. However, the conformational dynamics we observed probably facilitate the major structural change leading to opening of the substrate binding site. Indeed, dynamic loops important for nucleosome binding have been characterized in a variety of chromatin-interacting domains, such as the Sir3 BAH domain,[46] the PCAF/GCN5 histone acetyltransferase,[47] and bromodomains.[48] For example, multiple crystal structures of the Sir3 BAH domain showed that residues in two flexible loops are completely disordered in the free BAH domain structure,[49,50] but these residues become ordered or partially ordered upon binding to nucleosomes.[46]

We also found that *in vitro* ASH1L is much more active on native nucleosomes than on recombinant nucleosomes. Furthermore, ASH1L constructs including chromatin binding domains have significantly enhanced activity compared to that of the isolated SET domain. Together, these findings suggest a model whereby chromatin binding domains of ASH1L recognize posttranslational modifications on native nucleosomes and facilitate catalytic activity of the SET domain via substrate recruitment. Interestingly, the results of Eram et al. showing enhanced activity of the isolated ASH1L SET domain on native nucleosomes[8] suggest that the SET domain itself may also have increased affinity for native nucleosomes. In previous studies, ASH1L has been reported to methylate both H3K4 and H3K36.[2−8] While the precise targets of ASH1L *in vivo* are still under investigation, such promiscuity suggests that ASH1L specificity depends on the nature of the substrate, similar to the NSD family.[51] The number of methyl groups transferred by ASH1L is an additional unanswered question with important implications for the control of gene expression. In an *in vitro* enzyme assay, ASH1L can mono- and dimethylate, but not trimethylate, H3K36.[8] On the other hand, there is *in vivo* evidence in mouse that ASH1L may trimethylate H3K36.[6] The autoinhibitory loop may function to regulate the number of methyl groups transferred, because the Q2265A mutation leads to H3K36me3 in addition to the original H3K36me2 product.[7]

In summary, we discovered concerted dynamics in two loops of the ASH1L SET domain and showed that these loops regulate ASH1L enzymatic activity. Conformational dynamics in the substrate binding region of ASH1L may create transient pockets into which small molecule ligands could bind. Thus, it may be feasible to exploit the conformational dynamics to design small molecule inhibitors of ASH1L.

■ ASSOCIATED CONTENT

Supporting Information

The Supporting Information is available free of charge on the ACS Publications website at DOI: 10.1021/acs.biochem.5b00697.

Stereoview of mutagenesis sites in Figure 3E (Figure S1) (PDF)

■ AUTHOR INFORMATION

Corresponding Author

*Department of Pathology, University of Michigan, 1150 W. Medical Center Dr., MSRB I, Room 4510C, Ann Arbor, MI 48109. E-mail: tomaszc@umich.edu. Telephone: (734) 615-9324.

Funding

This work was supported by National Institutes of Health (NIH) Grant R01 (1R01CA160467) to J.G., a Leukemia and Lymphoma Society (LLS) TRP grants (6111-14 and 6485-16) to T.C., LLS Scholar Award 1215-14 to J.G., American Cancer Society Research Scholar Award RSG-13-130-01-CDD to J.G., and LLS Scholar Award 1227-14 to I.M. Use of the Advanced Photon Source was supported by the U.S. Department of Energy, Office of Science, Office of Basic Energy Sciences, under Contract DE-AC02-06CH11357. Use of LS-CAT Sector 21 was supported by the Michigan Economic Development Corp. and the Michigan Technology Tri-Corridor (Grant 085P1000817). D.S.R. acknowledges training grant support from the University of Michigan Chemistry-Biology Interface (CBI) training program (NIH Grant 5T32GM008597) and from the University of Michigan Medical Scientist Training Program (NIH Grant 5T32GM007863).

Notes

The authors declare no competing financial interest.

■ ACKNOWLEDGMENTS

We thank Yali Dou and Bo Zhou for assistance with recombinant nucleosome reconstitution, Carrie Johnson for critical reading of the manuscript, and members of the Grembecka and Cierpicki laboratories for many helpful discussions.

DOI: 10.1021/acs.biochem.5b00697
Biochemistry 2015, 54, 5401−5413

■ ABBREVIATIONS

ASH1L, absent, small, or homeotic-like 1; HMTase, histone methyltransferase; SET, Su(var.)3-9, enhancer-of-zeste, and trithorax; AWS, associated with the SET subdomain; SET-I, SET insertion subdomain; PHD, plant homeodomain; BAH, bromo-associated homology domain; SAM, *S*-adenosylmethionine; HSQC, heteronuclear single-quantum coherence; TROSY, transverse relaxation-optimized spectroscopy.

■ REFERENCES

(1) Tripoulas, N., LaJeunesse, D., Gildea, J., and Shearn, A. (1996) The Drosophila ash1 gene product, which is localized at specific sites on polytene chromosomes, contains a SET domain and a PHD finger. *Genetics 143*, 913−928.

(2) Gregory, G. D., Vakoc, C. R., Rozovskaia, T., Zheng, X., Patel, S., Nakamura, T., Canaani, E., and Blobel, G. A. (2007) Mammalian ASH1L is a histone methyltransferase that occupies the transcribed region of active genes. *Mol. Cell. Biol. 27*, 8466−8479.

(3) Xia, M., Liu, J., Wu, X., Liu, S., Li, G., Han, C., Song, L., Li, Z., Wang, Q., Wang, J., Xu, T., and Cao, X. (2013) Histone methyltransferase Ash1l suppresses interleukin-6 production and inflammatory autoimmune diseases by inducing the ubiquitin-editing enzyme A20. *Immunity 39*, 470−481.

(4) Tanaka, Y., Katagiri, Z.-I., Kawahashi, K., Kioussis, D., and Kitajima, S. (2007) Trithorax-group protein ASH1 methylates histone H3 lysine 36. *Gene 397*, 161−168.

(5) Yuan, W., Xu, M., Huang, C., Liu, N., Chen, S., and Zhu, B. (2011) H3K36 methylation antagonizes PRC2-mediated H3K27 methylation. *J. Biol. Chem. 286*, 7983−7989.

(6) Miyazaki, H., Higashimoto, K., Yada, Y., Endo, T. a., Sharif, J., Komori, T., Matsuda, M., Koseki, Y., Nakayama, M., Soejima, H., Handa, H., Koseki, H., Hirose, S., and Nishioka, K. (2013) Ash1l Methylates Lys36 of Histone H3 Independently of Transcriptional Elongation to Counteract Polycomb Silencing. *PLoS Genet. 9*, e1003897.

(7) An, S., Yeo, K. J., Jeon, Y. H., and Song, J. J. (2011) Crystal structure of the human histone methyltransferase ASH1L catalytic domain and its implications for the regulatory mechanism. *J. Biol. Chem. 286*, 8369−8374.

(8) Eram, M. S., Kuznetsova, E., Li, F., Lima-Fernandes, E., Kennedy, S., Chau, I., Arrowsmith, C. H., Schapira, M., and Vedadi, M. (2015) Kinetic characterization of human histone H3 lysine 36 methyltransferases, ASH1L and SETD2. *Biochim. Biophys. Acta, Gen. Subj. 1850*, 1842−1848.

(9) Liu, L., Kimball, S., Liu, H., Holowatyj, A., and Yang, Z.-Q. (2014) Genetic alterations of histone lysine methyltransferases and their significance in breast cancer. *Oncotarget 6*, 2466−2482.

(10) Colamaio, M., Puca, F., Ragozzino, E., Gemei, M., Decaussin-Petrucci, M., Aiello, C., Bastos, A. U., Federico, A., Chiappetta, G., Del Vecchio, L., Torregrossa, L., Battista, S., and Fusco, A. (2015) miR-142−3p downregulation contributes to thyroid follicular tumorigenesis by targeting ASH1L and MLL1. *J. Clin. Endocrinol. Metab. 100*, E59−E69.

(11) Gao, J., Aksoy, B. A., Dogrusoz, U., Dresdner, G., Gross, B., Sumer, S. O., Sun, Y., Jacobsen, A., Sinha, R., Larsson, E., Cerami, E., Sander, C., and Schultz, N. (2013) Integrative analysis of complex cancer genomics and clinical profiles using the cBioPortal. *Sci. Signaling 6*, pl1.

(12) Cerami, E., Gao, J., Dogrusoz, U., Gross, B. E., Sumer, S. O., Aksoy, B. A., Jacobsen, A., Byrne, C. J., Heuer, M. L., Larsson, E., Antipin, Y., Reva, B., Goldberg, A. P., Sander, C., and Schultz, N. (2012) The cBio cancer genomics portal: an open platform for exploring multidimensional cancer genomics data. *Cancer Discovery 2*, 401−404.

(13) Oh, H. R., An, C. H., Yoo, N. J., and Lee, S. H. (2014) Somatic mutations of amino acid metabolism-related genes in gastric and colorectal cancers and their regional heterogeneity - a short report. *Cell. Oncol. 37*, 455−461.

(14) Mouradov, D., Sloggett, C., Jorissen, R. N., Love, C. G., Li, S., Burgess, A. W., Arango, D., Strausberg, R. L., Buchanan, D., Wormald, S., O'Connor, L., Wilding, J. L., Bicknell, D., Tomlinson, I. P. M., Bodmer, W. F., Mariadason, J. M., and Sieber, O. M. (2014) Colorectal cancer cell lines are representative models of the main molecular subtypes of primary cancer. *Cancer Res. 74*, 3238−3247.

(15) Song, Y., Li, L., Ou, Y., Gao, Z., Li, E., Li, X., Zhang, W., Wang, J., Xu, L., Zhou, Y., Ma, X., Liu, L., Zhao, Z., Huang, X., Fan, J., Dong, L., Chen, G., Ma, L., Yang, J., Chen, L., He, M., Li, M., Zhuang, X., Huang, K., Qiu, K., Yin, G., Guo, G., Feng, Q., Chen, P., Wu, Z., Wu, J., Ma, L., Zhao, J., Luo, L., Fu, M., Xu, B., Chen, B., Li, Y., Tong, T., Wang, M., Liu, Z., Lin, D., Zhang, X., Yang, H., Wang, J., and Zhan, Q. (2014) Identification of genomic alterations in oesophageal squamous cell cancer. *Nature 509*, 91−95.

(16) Liu, J., Lee, W., Jiang, Z., Chen, Z., Jhunjhunwala, S., Haverty, P. M., Gnad, F., Guan, Y., Gilbert, H. N., Stinson, J., Klijn, C., Guillory, J., Bhatt, D., Vartanian, S., Walter, K., Chan, J., Holcomb, T., Dijkgraaf, P., Johnson, S., Koeman, J., Minna, J. D., Gazdar, A. F., Stern, H. M., Hoeflich, K. P., Wu, T. D., Settleman, J., de Sauvage, F. J., Gentleman, R. C., Neve, R. M., Stokoe, D., Modrusan, Z., Seshagiri, S., Shames, D. S., and Zhang, Z. (2012) Genome and transcriptome sequencing of lung cancers reveal diverse mutational and splicing events. *Genome Res. 22*, 2315−2327.

(17) Tanaka, Y., Kawahashi, K., Katagiri, Z. I., Nakayama, Y., Mahajan, M., and Kioussis, D. (2011) Dual function of histone H3 lysine 36 methyltransferase ASH1 in regulation of hox gene expression. *PLoS One 6*, e28171.

(18) Jones, M., Chase, J., Brinkmeier, M., Xu, J., Weinberg, D. N., Schira, J., Friedman, A., Malek, S., Grembecka, J., Cierpicki, T., Dou, Y., Camper, S. A., and Maillard, I. (2015) Ash1l controls quiescence and self-renewal potential in hematopoietic stem cells. *J. Clin. Invest. 125*, 2007−2020.

(19) Shah, N., and Sukumar, S. (2010) The Hox genes and their roles in oncogenesis. *Nat. Rev. Cancer 10*, 361−371.

(20) Zeisig, B. B., Milne, T., García-Cuéllar, M.-P., Schreiner, S., Martin, M.-E., Fuchs, U., Borkhardt, A., Chanda, S. K., Walker, J., Soden, R., Hess, J. L., and Slany, R. K. (2004) Hoxa9 and Meis1 are key targets for MLL-ENL-mediated cellular immortalization. *Mol. Cell. Biol. 24*, 617−628.

(21) Xiao, B., Jing, C., Kelly, G., Walker, P. A., Muskett, F. W., Frenkiel, T. A., Martin, S. R., Sarma, K., Reinberg, D., Gamblin, S. J., and Wilson, J. R. (2005) Specificity and mechanism of the histone methyltransferase Pr-Set7. *Genes Dev. 19*, 1444−1454.

(22) Qiao, Q., Li, Y., Chen, Z., Wang, M., Reinberg, D., and Xu, R.-M. (2011) The structure of NSD1 reveals an autoregulatory mechanism underlying histone H3K36 methylation. *J. Biol. Chem. 286*, 8361−8368.

(23) Zheng, W., Ibáñez, G., Wu, H., Blum, G., Zeng, H., Dong, A., Li, F., Hajian, T., Allali-Hassani, A., Amaya, M. F., Siarheyeva, A., Yu, W., Brown, P. J., Schapira, M., Vedadi, M., Min, J., and Luo, M. (2012) Sinefungin derivatives as inhibitors and structure probes of protein lysine methyltransferase SETD2. *J. Am. Chem. Soc. 134*, 18004−18014.

(24) Otwinowski, Z., and Minor, W. (1997) Processing of X-ray Diffraction Data Collected in Oscillation Mode. In *Methods in Enzymology* (Carter, C. W., Jr., and Sweet, R. M., Eds.) pp 307−326, Academic Press, New York.

(25) Vagin, A., and Teplyakov, A. (1997) MOLREP: an Automated Program for Molecular Replacement. *J. Appl. Crystallogr. 30*, 1022−1025.

(26) Murshudov, G. N., Skubák, P., Lebedev, A. A., Pannu, N. S., Steiner, R. A., Nicholls, R. A., Winn, M. D., Long, F., and Vagin, A. A. (2011) REFMAC5 for the refinement of macromolecular crystal structures. *Acta Crystallogr., Sect. D: Biol. Crystallogr. 67*, 355−367.

(27) Emsley, P., Lohkamp, B., Scott, W. G., and Cowtan, K. (2010) Features and development of Coot. *Acta Crystallogr., Sect. D: Biol. Crystallogr. 66*, 486−501.

(28) Winn, M. D., Ballard, C. C., Cowtan, K. D., Dodson, E. J., Emsley, P., Evans, P. R., Keegan, R. M., Krissinel, E. B., Leslie, A. G. W., McCoy, A., McNicholas, S. J., Murshudov, G. N., Pannu, N. S.,

DOI: 10.1021/acs.biochem.5b00697
Biochemistry 2015, 54, 5401−5413

Potterton, E. A., Powell, H. R., Read, R. J., Vagin, A., and Wilson, K. S. (2011) Overview of the CCP4 suite and current developments. *Acta Crystallogr., Sect. D: Biol. Crystallogr. 67*, 235−242.
(29) Chen, V. B., Arendall, W. B., Headd, J. J., Keedy, D. A., Immormino, R. M., Kapral, G. J., Murray, L. W., Richardson, J. S., and Richardson, D. C. (2010) MolProbity: all-atom structure validation for macromolecular crystallography. *Acta Crystallogr., Sect. D: Biol. Crystallogr. 66*, 12−21.
(30) Schneider, B., Gelly, J. C., de Brevern, A. G., and Černý, J. (2014) Local dynamics of proteins and DNA evaluated from crystallographic B factors. *Acta Crystallogr., Sect. D: Biol. Crystallogr. 70*, 2413−2419.
(31) Delaglio, F., Grzesiek, S., Vuister, G. W., Zhu, G., Pfeifer, J., and Bax, A. (1995) NMRPipe: a multidimensional spectral processing system based on UNIX pipes. *J. Biomol. NMR 6*, 277−293.
(32) Goddard, T. D., and Kneller, D. G. (2008) *SPARKY 3*, University of California, San Francisco.
(33) Hardman, C. H., Broadhurst, R. W., Raine, A. R. C., Grasser, K. D., Thomas, J. O., and Laue, E. D. (1995) Structure of the A-Domain of HMG1 and Its Interaction with DNA as Studied by Heteronuclear Three- and Four-Dimensional NMR Spectroscopy. *Biochemistry 34*, 16596−16607.
(34) Shim, Y., Duan, M.-R., Chen, X., Smerdon, M. J., and Min, J.-H. (2012) Polycistronic coexpression and nondenaturing purification of histone octamers. *Anal. Biochem. 427*, 190−192.
(35) Kleckner, I. R., and Foster, M. P. (2011) An introduction to NMR-based approaches for measuring protein dynamics. *Biochim. Biophys. Acta, Proteins Proteomics 1814*, 942−968.
(36) Bain, A. D. (2003) Chemical exchange in NMR. *Prog. Nucl. Magn. Reson. Spectrosc. 43*, 63−103.
(37) Shi, J., and Vakoc, C. R. (2014) The Mechanisms behind the Therapeutic Activity of BET Bromodomain Inhibition. *Mol. Cell 54*, 728−736.
(38) Ali, M., Hom, R. A., Blakeslee, W., Ikenouye, L., and Kutateladze, T. G. (2014) Diverse functions of PHD fingers of the MLL/KMT2 subfamily. *Biochim. Biophys. Acta, Mol. Cell Res. 1843*, 366−371.
(39) Chambers, A. L., Pearl, L. H., Oliver, A. W., and Downs, J. a. (2013) The BAH domain of Rsc2 is a histone H3 binding domain. *Nucleic Acids Res. 41*, 9168−9182.
(40) Heerboth, S., Lapinska, K., Snyder, N., Leary, M., Rollinson, S., and Sarkar, S. (2014) Use of Epigenetic Drugs in Disease: An Overview. *Genet. Epigenet. 2014*, 9−19.
(41) Couture, J.-F., Collazo, E., Brunzelle, J. S., and Trievel, R. C. (2005) Structural and functional analysis of SET8, a histone H4 Lys-20 methyltransferase. *Genes Dev. 19*, 1455−1465.
(42) Xiao, B., Jing, C., Wilson, J. R., Walker, P. A., Vasisht, N., Kelly, G., Howell, S., Taylor, I. A., Blackburn, G. M., and Gamblin, S. J. (2003) Structure and catalytic mechanism of the human histone methyltransferase SET7/9. *Nature 421*, 652−656.
(43) Trievel, R. C., Flynn, E. M., Houtz, R. L., and Hurley, J. H. (2003) Mechanism of multiple lysine methylation by the SET domain enzyme Rubisco LSMT. *Nat. Struct. Biol. 10*, 545−552.
(44) Zhang, X., Yang, Z., Khan, S. I., Horton, J. R., Tamaru, H., Selker, E. U., and Cheng, X. (2003) Structural basis for the product specificity of histone lysine methyltransferases. *Mol. Cell 12*, 177−185.
(45) Xiao, B., Wilson, J. R., and Gamblin, S. J. (2003) SET domains and histone methylation. *Curr. Opin. Struct. Biol. 13*, 699−705.
(46) Armache, K.-J., Garlick, J. D., Canzio, D., Narlikar, G. J., and Kingston, R. E. (2011) Structural basis of silencing: Sir3 BAH domain in complex with a nucleosome at 3.0 Å resolution. *Science 334*, 977−982.
(47) Zheng, Y., Mamdani, F., Toptygin, D., Brand, L., Stivers, J. T., and Cole, P. A. (2005) Fluorescence analysis of a dynamic loop in the PCAF/GCN5 histone acetyltransferase. *Biochemistry 44*, 10501−10509.
(48) Steiner, S., Magno, A., Huang, D., and Caflisch, A. (2013) Does bromodomain flexibility influence histone recognition? *FEBS Lett. 587*, 2158−2163.
(49) Hou, Z., Danzer, J. R., Fox, C. A., and Keck, J. L. (2006) Structure of the Sir3 protein bromo adjacent homology (BAH) domain from S. cerevisiae at 1.95 A resolution. *Protein Sci. 15*, 1182−1186.
(50) Connelly, J. J., Yuan, P., Hsu, H.-C., Li, Z., Xu, R.-M., and Sternglanz, R. (2006) Structure and function of the Saccharomyces cerevisiae Sir3 BAH domain. *Mol. Cell. Biol. 26*, 3256−3265.
(51) Li, Y., Trojer, P., Xu, C.-F., Cheung, P., Kuo, A., Drury, W. J., Qiao, Q., Neubert, T. A., Xu, R.-M., Gozani, O., and Reinberg, D. (2009) The target of the NSD family of histone lysine methyltransferases depends on the nature of the substrate. *J. Biol. Chem. 284*, 34283−34295.
(52) Karplus, P. A., and Diederichs, K. (2012) Linking crystallographic model and data quality. *Science 336*, 1030−3.

DOI: 10.1021/acs.biochem.5b00697
Biochemistry 2015, 54, 5401−5413